



**HAL**  
open science

# Anisotropic dense collagen hydrogels with two ranges of porosity to mimic the skeletal muscle extracellular matrix

Marie Camman, Pierre Joanne, Julie Brun, Alba Marcellan, Julien Dumont, Onnik Agbulut, Christophe H elary

## ► To cite this version:

Marie Camman, Pierre Joanne, Julie Brun, Alba Marcellan, Julien Dumont, et al.. Anisotropic dense collagen hydrogels with two ranges of porosity to mimic the skeletal muscle extracellular matrix. *Biomaterials Advances*, 2023, 144, pp.213219. 10.1016/j.bioadv.2022.213219 . hal-03894624

**HAL Id: hal-03894624**

**<https://hal.sorbonne-universite.fr/hal-03894624>**

Submitted on 12 Dec 2022

**HAL** is a multi-disciplinary open access archive for the deposit and dissemination of scientific research documents, whether they are published or not. The documents may come from teaching and research institutions in France or abroad, or from public or private research centers.

L'archive ouverte pluridisciplinaire **HAL**, est destin ee au d ep ot et  a la diffusion de documents scientifiques de niveau recherche, publi es ou non,  emanant des  tablissements d'enseignement et de recherche fran ais ou  trangers, des laboratoires publics ou priv es.

# **Anisotropic dense collagen hydrogels with two ranges of porosity to mimic the skeletal muscle extracellular matrix**

Marie Camman<sup>1,2</sup>, Pierre Joanne<sup>2</sup>, Julie Brun<sup>3</sup>, Alba Marcellan<sup>3</sup>, Julien Dumont<sup>4</sup>, Onnik Agbulut<sup>2\*</sup>, Christophe H elary<sup>1\*</sup>

<sup>1</sup> Laboratoire de Chimie de la Mati ere Condens ee de Paris, Sorbonne Universit e, CNRS, UMR 7574, F-75005, Paris, France.

<sup>2</sup> Institut de Biologie Paris-Seine (IBPS), Sorbonne Universit e, CNRS, UMR 8256, Inserm U1164, Biological Adaptation and Ageing, F-75005, Paris, France.

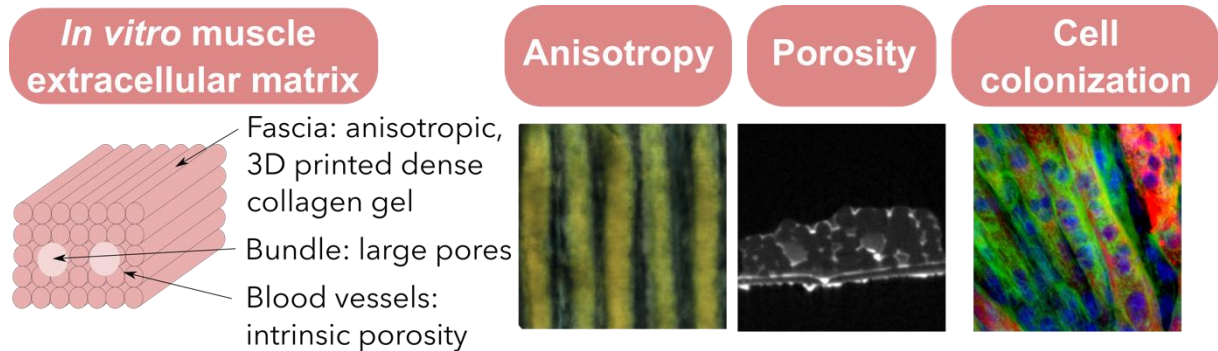
<sup>3</sup> Sciences et Ing enierie de la Mati ere Molle, ESPCI Paris, Universit e PSL, CNRS, Sorbonne Universit e, F-75005, Paris, France.

<sup>4</sup> CIRB Microscopy facility, Coll ege de France, CNRS, UMR 7241, Inserm U1050, F-75005, Paris, France.

\* Corresponding authors: Christophe H elary and Onnik Agbulut  
Email address : [christophe.helary@sorbonne-universite.fr](mailto:christophe.helary@sorbonne-universite.fr) & [onnik.agbulut@sorbonne-universite.fr](mailto:onnik.agbulut@sorbonne-universite.fr)

Postal address: Sorbonne University - Campus Pierre et Marie Curie, 4 place Jussieu, 75252 Paris Cedex 05, France

## Graphical Abstract



## Highlights

- Design of a novel extracellular matrix-like hydrogel to enhance the physiological relevance of skeletal muscle models.
- Porous and anisotropic dense collagen hydrogels mimic the physical properties of the extracellular matrix of muscle tissue.
- Unidirectional printing of dense collagen creates a porous and anisotropic scaffold in a single step.
- Anisotropic dense collagen hydrogels promote skeletal myoblast differentiation into myotubes and their 3D organization.

## ABSTRACT

Despite the crucial role of the extracellular matrix (ECM) in the organotypic organization and function of skeletal muscles, most 3D models do not mimic its specific characteristics, namely its biochemical composition, stiffness, anisotropy, and porosity. Here, a novel 3D *in vitro* model of muscle ECM was developed reproducing these four crucial characteristics of the native ECM. An anisotropic hydrogel mimicking the muscle fascia was obtained thanks to unidirectional 3D printing of dense collagen with aligned collagen fibrils. The space between the different layers was tuned to generate an intrinsic network of pores (100  $\mu\text{m}$ ) suitable for nutrient and oxygen diffusion. By modulating the gelling conditions, the mechanical properties of the construct reached those measured in the physiological muscle ECM. This artificial matrix was thus evaluated for myoblast differentiation. The addition of large channels (600  $\mu\text{m}$ ) by molding permitted to create a second range of porosity suitable for cell colonization without altering the physical properties of the hydrogel. Skeletal myoblasts embedded in Matrigel®, seeded within the channels, organized in 3D, and differentiated into multinucleated myotubes. These results show that porous and anisotropic dense collagen hydrogels are promising biomaterials to model skeletal muscle ECM.

**Keywords:** Muscle extracellular matrix, dense collagen, 3D printing, anisotropy, porosity

## 1. Introduction

Skeletal muscles are involved in the body locomotion thanks to their highly organized tridimensional structure. The epimysium is a connective tissue surrounding the whole skeletal muscle. The perimysium, consisting of aligned collagen I fibers (anisotropy), separates each muscle bundle of myofibers [1]. These two matrices are part of the muscle fascia. Inside, the myofibers are highly aligned and densely packed within a loose connective tissue called endomysium. This latter resembles a basal membrane composed of collagen IV, fibronectin, and laminin [2]. This hierarchical organization is fundamental for muscle contraction and the integrity of the neuromuscular junction [3].

Because of its high complexity, the first *in vitro* models of skeletal muscle were limited to monolayers of myoblasts cultured on a petri dish coated with Matrigel® [4–6]. Matrigel reproduced the endomysium's biochemical cues and helped myoblasts to grow and differentiate. However, these 2D models did not reproduce the 3D muscle organization. 3D *in vitro* microtissues overcome these limitations by reproducing the cellular microenvironment. The most popular 3D models rely on encapsulating muscle cells within soft hydrogels made of fibrin, collagen, or gelatin between anchors [7–9]. Myoblasts align along the axis of the hydrogel due to cell contraction and create a displacement of the anchors. The primary readout of such a model is contractility. In these systems, the properties (stiffness and topography) of the muscular extracellular matrix (ECM), which are crucial in the muscle function for the force transmission, are not considered. In addition, hydrogels are not stable, and a necrotic core appears due to the absence of porosity [10].

The ideal biomaterial mimicking the physiological ECM (fascia) surrounding the muscle bundles should be composed of 2-5 % (w/v) collagen I [11], be anisotropic and have high mechanical properties ( $E=12$  kPa). In addition, this ECM should be porous to ensure nutrient diffusion [12] and allow cell survival.

Most of the current models used synthetic or natural polymers but rarely collagen. This choice can be explained by the multiple drawbacks of collagen hydrogels when made from low concentrated solutions (0.5% wt): poor mechanical stiffness inducing shrinkage when colonized with cells [13].

Anisotropy of the muscle ECM is crucial to guide myofibers and allows their alignment *in vivo*. Mimicking the topography of the fascia *in vitro* allows the control of the organotypic organization and the cell phenotype. Collagen anisotropy at sample scale can be obtained by electrospinning or under a high magnetic field [14–18]. Besides, anisotropic collagen threads can be produced by extruding dense collagen solutions within a gelling bath made of PBS 5X [19] or other buffers [20]. The high ionic strength and the neutral pH of PBS 5X are required to trigger fibrillogenesis and collagen gelling without addition of any chemical cross-linking. In addition, PBS 5X prevents swelling. Alternatively, anisotropic layers or gels can be obtained by 3D printing [21–23]. These strategies create oriented collagen fibrils (anisotropy) suitable for cell culture. However, they are not biomimetic 3D models when cells are seeded on top of the construct, *i.e.*, not organized in densely packed bundles within the threads [24,25].

A significant limitation of 3D models is the slow diffusion of nutrients and oxygen, leading to the formation of a necrotic core [26]. Hence, porosity is an important feature to consider for cell survival maintenance. Several strategies, such as porogen leaching or self-assembly, have increased nutrient diffusion but require solvents or modified collagen. Additionally, pore geometry is barely controllable [27,28]. 3D printing can create an intrinsic porosity by stacking round filaments [29–31]. However, the 90° switch between layers disturbs anisotropy and the channel shape, limiting its utilization.

Other techniques, such as needle or suture thread molding, generate topological anisotropy with large and elongated channels suitable for cell colonization and differentiation into

myotubes (>500  $\mu\text{m}$ ) [29,32–34]. This kind of porosity is challenging to obtain by 3D printing due to the channel collapsing. Unfortunately, it is also difficult to multiply the number of needles to dedicate one fraction for nutrient diffusion beside channels for cell colonization.

Hence, an artificial muscle ECM with the appropriate physicochemical cues and suitable mechanical properties has not been described yet. In addition, collagen biomaterials presenting two sets of porosity (for cell colonization and perfusion) have not been designed either.

In this study, we aimed to design a novel *in vitro* 3D model mimicking the physical properties and the structure of the skeletal muscle ECM. For this purpose, its key features (biochemical cues, stiffness, porosity, anisotropy) were set within a single hydrogel using 3D printing. Collagen fibrillogenesis and gelling were performed using different procedures in order to optimize the fibril and porosity size together with the hydrogel properties. Then C2C12 cells, used as muscle cell model, were seeded in 3D in Matrigel® to form bundles inside the large channels of 3D printed hydrogels.

## **2. Materials and Methods**

### *2.1. Solutions preparation*

PBS 5X solution was prepared with 680 mM NaCl, 40 mM  $\text{Na}_2\text{HPO}_4 \cdot 12 \text{H}_2\text{O}$ , 13 mM KCl and 8 mM  $\text{NaH}_2\text{PO}_4 \cdot 1 \text{H}_2\text{O}$  (all products were obtained from Sigma). PBS 1X was obtained by diluting 1:5 PBS 5X in distilled water. Ammonium hydroxide 30 % (v/v) (CarloErba) was poured in a beaker inside a dessicator to generate vapors.

### *2.2. Collagen extraction and purification*

As previously described, type I collagen was extracted and purified from rat tail tendons [35]. Briefly, rat tails were rinsed with ethanol 70% and cut into small pieces of 1 cm to extract tendons. Tendons were solubilized in 500 mM acetic acid (Carlo Erba). After precipitation with 0.7 M NaCl (Sigma), centrifugation, and dialysis, collagen purity was observed after SDS-PAGE electrophoresis (MiniProtean TGX, Biorad), and its concentration was estimated by hydroxyproline titration [35]. After an evaporation step in a safety cabinet for several days, collagen solutions concentrated at  $30 \text{ mg}\cdot\text{mL}^{-1}$  (3 % w/v) in acetic acid were obtained. Finally, collagen solutions were stored at  $4^\circ\text{C}$  before utilization.

### *2.3. Collagen 3D printing*

3D printing was performed using a home-built 3D printer. The concentrated collagen solution was poured into a 1 mL syringe (Terumo) with a flat bottom 23G needle (inner diameter  $330 \mu\text{m}$ ). A unique layer of  $10 \text{ mm} \times 5 \text{ mm} \times 0.33 \text{ mm}$  was designed using the AutoDesk Fusion 360 software. The 3D file (.stl) was then sliced with Repetier software with a rectilinear pattern to obtain unidirectional lines inside the square. This layer was printed and repeated at different z 5 times to form a 5-layered collagen construct with all filaments oriented in the same direction. The extrusion speed was optimal at  $2 \text{ mm}\cdot\text{s}^{-1}$  (extrusion rate  $1 \mu\text{l}\cdot\text{s}^{-1}$ ). The filling was set to 100% to ensure cohesiveness between every filament but the interlayer gap varied between  $300$  and  $500 \mu\text{m}$  to tune the hydrogel porosity. Anisotropy was induced by collagen shearing during extrusion, and this anisotropy was maintained by printing into a PBS 5X bath. The negative control was printed in air and gelled with ammonia vapors. The printing process lasted less than 10 minutes (1 min 30 sec per layer).

### *2.4. Collagen gelling and fibrillogenesis after 3D printing*



Different strategies were tested to extend the collagen gelling and maintain the anisotropy while setting high mechanical properties. After the printing step inside PBS 5X, hydrogels were left in a large amount of PBS 5X to continue the initial gelling at pH 7.4 with high ionic strength (from 30 min to 7 days). At the end of this period, some collagen constructs were exposed to ammonia vapors for 24 hours to increase gelation. For this purpose, an ammonium hydroxide solution (30 % (v/v) Carlo Erba) was poured into a glass beaker and placed in a desiccator. Constructs only gelled by ammonia vapors were printed in air and directly placed inside the desiccator for 1 day. After ammonia vapors, collagen constructs were rinsed several times in PBS 1X baths until a neutral pH was reached (at least 24 hours). Gelling conditions are presented in Table 1. Casted gels with the same gelling conditions were carried out as negative controls.

<b>Gelling and Fibrillogenesis Conditions</b>	<b>Initial gelling</b>	<b>Extended gelling</b>	
	<b>Printing bath (PBS 5X)</b>	<b>Time in PBS 5X</b>	<b>Time under ammonia vapors</b>
1 day NH <sub>3</sub>	No	-	1 day
30 min PBS/1 day NH <sub>3</sub>	Yes	30 min	1 day
1 day PBS/1 day NH <sub>3</sub>	Yes	1 day	1 day
6 days PBS/1 day NH <sub>3</sub>	Yes	6 days	1 day
1 day PBS	Yes	1 day	-
7 days PBS	Yes	7 days	-

**Table 1.** Printing conditions and gelation process.

### 2.5. X-Ray Microtomography (Micro-CT) analysis

This technique aimed to monitor the internal structure of collagen hydrogels. Gels were loaded with Micropaque contrast agent (Guerbet) before their observation and scanned using a high-resolution X-ray micro-CT system (Quantum FX Caliper, Life Sciences, Perkin Elmer, Waltham, MA, United States) hosted by the PIV Platform (UR2496, Montrouge, France). The contrast agent appeared white when imaged and collagen filaments were black. Standard acquisition settings were applied (voltage 90 kV, intensity 160 mA), and scans were performed with a field of view of 1 cm<sup>2</sup>. Micro-CT datasets were analyzed using the built-in multiplanar reconstruction tool, Osirix Lite (Pixmeo, Switzerland), to obtain time series of

images and 3D reconstruction. Micro-CT images were thus analyzed using Image J. Images were thresholded and the diameter of the pores were measured. The irregular shape of the pores was captured using different parameters such as the Feret min diameter (the largest circle that can be drawn within the pores), the Feret max diameter (the smallest circle that surrounds the pore), and circularity.

### *2.6. Second-harmonic generation (SHG)*

Second-harmonic generation microscopy was used to observe anisotropy as a strong SHG signal is proportional to collagen quantity and alignment. SHG images were acquired with a Mai Tai multiphoton laser-equipped confocal microscope (Leica SP8). SHG signal was collected with a hybrid detector between 430 and 450 nm (excitation at 880 nm). A long-distance objective (25X water immersion) was used to acquire z-stacks with optimal settings for each sample. Image series were acquired with the Leica Application Suite X software.

### *2.7. Polarized Light Microscopy*

Collagen anisotropy of 3D printed hydrogels was also analyzed by polarized light microscopy (PLM). PLM was performed using a photonic Nikon microscope equipped with crossed-polarizers to observe collagen birefringence. Collagen fibrils with uniaxial alignment will increase or decrease the light intensity depending on the relative orientation of the crossed polarizer to the sample. A series of images were acquired with multiple sample orientations to demonstrate the light intensity variation. Maxima and minima were separated by 45°. These observations were correlated with those obtained by SHG.

### *2.8. Rheological measurements*

Shear oscillatory measurements were performed on casted collagen hydrogels with different gelling parameters using an Anton Paar rheometer. An 8 mm parallel-plate geometry was fitted with a rough surface to avoid gel slipping. All measurements were performed at 37 °C. Storage modulus,  $G'$  and loss modulus,  $G''$  were recorded during a frequency sweep from 0.1 to 10 Hz with an imposed strain of 1 %. This strain corresponds to non-destructive conditions (linear viscoelastic regime) as previously checked (data not shown). The geometry and a stabilized normal force (0.01 N) were optimized. Three samples of each matrix were tested.

### *2.9. Tensile tests*

Mechanical tests were performed on printed gels with a tensile testing machine (Instron) equipped with a 10 N load cell and Bluehill software. Printed gels were obtained by printing 5 successive layers of 25 mm x 5 mm either in the longitudinal or transversal direction. Total thickness of the sample was around 1 mm (measured before each experiment). All experiments were performed on hydrated samples (three specimens per condition) at 21 °C at a constant strain rate of  $0.06 \text{ s}^{-1}$ . The elastic (Young's) modulus of collagen hydrogels was measured by a linear fit within the first 5 % deformation. The strain,  $e$  and stress,  $s$  were estimated as  $e = \Delta L / L$  ( $L$ =sample length) and  $s = F / S_0$  respectively. Cross-section area,  $S_0$ , was assumed to be homogeneous and calculated from the measure of the initial width and thickness.

### *2.10. Transmission Electron Microscopy (TEM)*

For one hour, collagen hydrogels were fixed using 3.63 % (w/v) glutaraldehyde (Electron Microscopy Sciences) in cacodylate/saccharose buffer (Sigma) (0.05 M/0.3 M, pH=7.4). Samples were washed three times in cacodylate/saccharose buffer (0.05 M/0.3 M, pH=7.4). Samples were colored with nuclear red for 1 hour before progressive dehydration through

increasing baths of ethanol from 30 % (v/v) to 100 % (v/v) and propylene oxide (Carlo Erba). Last, the hydrogels were embedded in Araldite. Araldite transverse ultra-thin sections (70 nm) were performed using a Leica EM UC7 ultramicrotome and contrasted with 0.5 % (w/v) uranyl acetate. Sections were then observed with a Cryo-microscope Tecnai spirit G2 electron microscope 214 operating at 120 kV. For each 3D-printed or cast hydrogel, photos were taken at a magnification of x15,000 with a 215 CCD Camera (Orius Gatan 832 digital) and analyzed.

### *2.11. Differential Scanning Calorimetry (DSC)*

10-20 mg of collagen hydrogel was placed into an aluminum pan. The reference was an empty pan. Measurements were acquired with a NanoScan Differential Scanning Calorimetry. A temperature scanning from 20°C to 100°C with a 10°C·min<sup>-1</sup> ramp was performed to detect the collagen fibril denaturation peak.

### *2.12. Fibroblast cell culture to observe collagen anisotropy*

Normal Human Dermal Fibroblasts (NHDF) were used for their ability to sense the substrate topography [36]. They are a living control for the anisotropy induced in the collagen constructs as they align along the longitudinal fibril axis. Briefly, they were cultured in a complete cell culture medium (Dulbecco's Modified Eagle's Medium (DMEM) supplemented with 10 % (v/v) fetal bovine serum, 100 U·mL<sup>-1</sup> penicillin, 100 µg·mL<sup>-1</sup> streptomycin, 0.25 µg·mL<sup>-1</sup> Fungizone, and Glutamax) for 48 hours. Then, they were trypsinized (with 0.1 % (v/v) trypsin and 0.02 % (v/v) EDTA), and 5,000 cells were seeded on top of collagen hydrogels and cultivated for one day to observe their alignment. After fixation with paraformaldehyde, 4 % (w/v) overnight at 4°C, and staining with Phalloidin Alexa fluor 488 nm (labeling F-actin), hydrogels were analyzed with SHG coupled with fluorescent

microscopy. Fibroblasts orientation along the collagen filaments was analyzed using the Orientation J plug-in (Fiji).

### *2.13. Pore generation*

Large channels were added to the scaffolds using needles. First, the hydrogels were printed into a PBS 5X bath or in the air (for the negative control) inside dedicated 3D-printed plastic molds with holes (10 x 5 x 1.5 mm). After 30 min of gelling inside PBS 5X, 2 needles (external diameter 600  $\mu\text{m}$ /23 G) were placed into the collagen scaffold through the dedicated holes of the mold. The fibrillogenesis and gelling processes were then continued. After complete gelling and a PBS 1X rinsing, needles were removed to reveal straight, well-defined channels that cross the whole hydrogel.

### *2.14. C2C12 culture inside large channels*

C2C12 were expanded in proliferation medium (DMEM high glucose, 20 % (v/v) fetal bovine serum, 100 U·mL<sup>-1</sup> penicillin, 100  $\mu\text{g}\cdot\text{mL}^{-1}$  streptomycin) until 50% confluency. They were trypsinized and amplified to avoid confluency.

To seed C2C12 into printed collagen hydrogels (1 day PBS/1 day NH<sub>3</sub>), cells were resuspended in Matrigel at 3·10<sup>7</sup> cells·mL<sup>-1</sup> (Sigma, Bioreagent) on ice. 3  $\mu\text{l}$  of cell suspension were injected with a P10 pipet in each channel created by needles (600  $\mu\text{m}$ ). After 24h, two conditions were used: a first group was left in proliferation medium for 4 or 7 days in culture, whereas the other group was cultivated during the same period with differentiation medium (DMEM high glucose, 2 % (v/v) horse serum, 100 U·mL<sup>-1</sup> penicillin, 100  $\mu\text{g}\cdot\text{mL}^{-1}$  streptomycin). The medium was changed every day. Constructs were then fixed in paraformaldehyde 4 % (w/v) (Sigma) in PBS 1X overnight at 4 °C and sectioned into 250  $\mu\text{m}$  slices with a vibratome. All experiments were carried out in triplicates.

### *2.15. Fluorescence and Second-Harmonic Generation microscopy*

For constructs colonized by C2C12, the fluorescent labeling of nuclei (TOPRO-3, Thermofisher) and F-actin filaments (Alexa Fluor 488 phalloidin, Thermofisher) were performed on 250  $\mu\text{m}$  sections containing the channels. Additional labeling of C2C12 with MF-20 hybridoma mouse IgG2B primary antibody and Alexa Fluor 546 goat anti-mouse IgG2B secondary antibody (Invitrogen) was used to evaluate the cell differentiation into myotubes. Observations were conducted with a Leica SP5 upright confocal, multiphoton laser scanning microscopy, which enabled the simultaneous acquisition of fluorescence and second-harmonic generation signals.

### *2.16. Statistical analysis*

All experiments were carried out at least twice, and the results were expressed as the mean values  $\pm$  standard deviation (SD). The differences were analyzed using Mann-Whitney test for paired comparisons or Kruskal-Wallis test for multiple comparisons.  $p < 0.05$  was considered significant.

## **3. Results**

### *3.1.3D printing of porous dense collagen hydrogels*

The home-built 3D printer enabled the printing of  $30 \text{ mg}\cdot\text{mL}^{-1}$  collagen solutions through a 23 G flat bottom needle, creating a constant flow of collagen solution to ensure a stable transport of the extrudate away from the printer. In addition, the collagen molecules aligned along the axis of the needle during the process (Figure 1-A) [19]. To obtain the optimal construct, suitable parameters such as printing speed, printing condition (air or PBS 5X), or height between two successive layers had to be optimized. First, the printing speed was varied from 1 to  $10 \text{ mm}\cdot\text{s}^{-1}$ , but  $2 \text{ mm}\cdot\text{s}^{-1}$  was chosen to obtain a homogeneous thread without

collagen excess. Then, the filament was either printed in a petri dish filled with PBS 5X (for all conditions except 1 day NH<sub>3</sub>) or in the air (for 1 day NH<sub>3</sub> gelling). The PBS 5X bath gelled quasi-instantaneously the collagen solution and allowed an excellent shape fidelity and reproducibility of the printing process. A 5 layered collagen hydrogel was obtained with all filaments oriented in the same direction (10 x 5 x 1.5 mm) (Figure 1-B and C). Finally, to tune the space between two layers, the same layer was repeated at different z-positions. Gelling kinetics in PBS 5X was founded to be the best compromise for a printing bath: sufficiently fast to preserve the round shape of filaments (and create intrinsic porosity between filaments) and slow enough to ensure their fusion, thereby ensuring the cohesiveness of the construct (Figure 2-A, B and C).

The generated pores depend on the space between each printed layer and can reach a diameter of 150 µm for the 500 µm interspace (Figure 2-G). The number of pores also depended on the interlayer space and was optimal for 400 µm (Figure 2-H) as many pores collapsed for 300 µm and 500 µm. The hydrogel cohesiveness decreased with a 500 µm interlayer space, and the well-organized stack was lost. This was observed experimentally by a decrease in height and organization on histological sections, explaining the decrease in pore circularity and the low number of open pores (Figure 2-H and I). From these different tests, the best combination between cohesiveness and porosity was found for an interspace of 400 µm between each layer, generating well-dispersed 100 µm intrinsic pores that cross the hydrogel from one side to the other (Figure S1 and S2). Following the printing process in the initial PBS 5X bath, the fibrillogenesis process was continued in PBS 5X or under ammonia vapors according to the different tested conditions (see Table 1). Once gelled, extensive washes in PBS 1X restored a neutral pH and/or an ionic strength compatible with cell culture, and constructs were stored in PBS 1X at 4 °C until use.

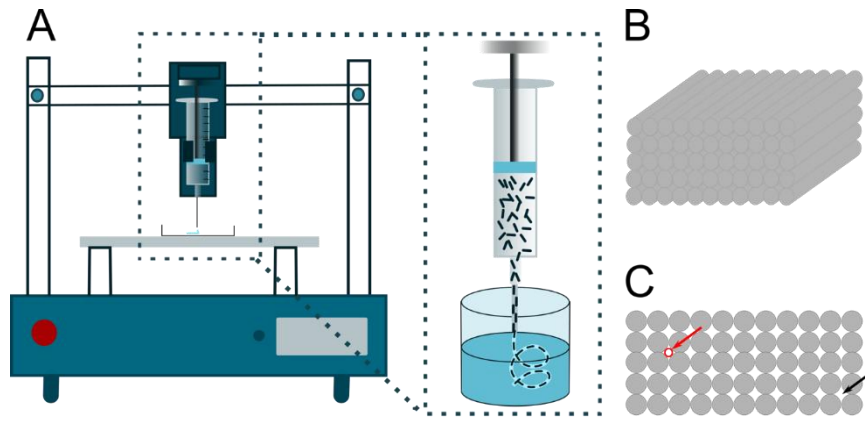


**Figure 1.** (A) 3D printing set up. The dense collagen solution was extruded through a 23G flat bottom needle. Collagen molecules aligned along the axis of the needle and the PBS 5X bath froze their anisotropic organization thanks to the rise in pH and the osmotic pressure. (B) 3D view and (C) Lateral view of the printed gel (gel dimension 1 cm x 1 cm x 2 mm). The black arrow indicates the interlayer space, and the red circle and arrow indicate the diameter of the pores.



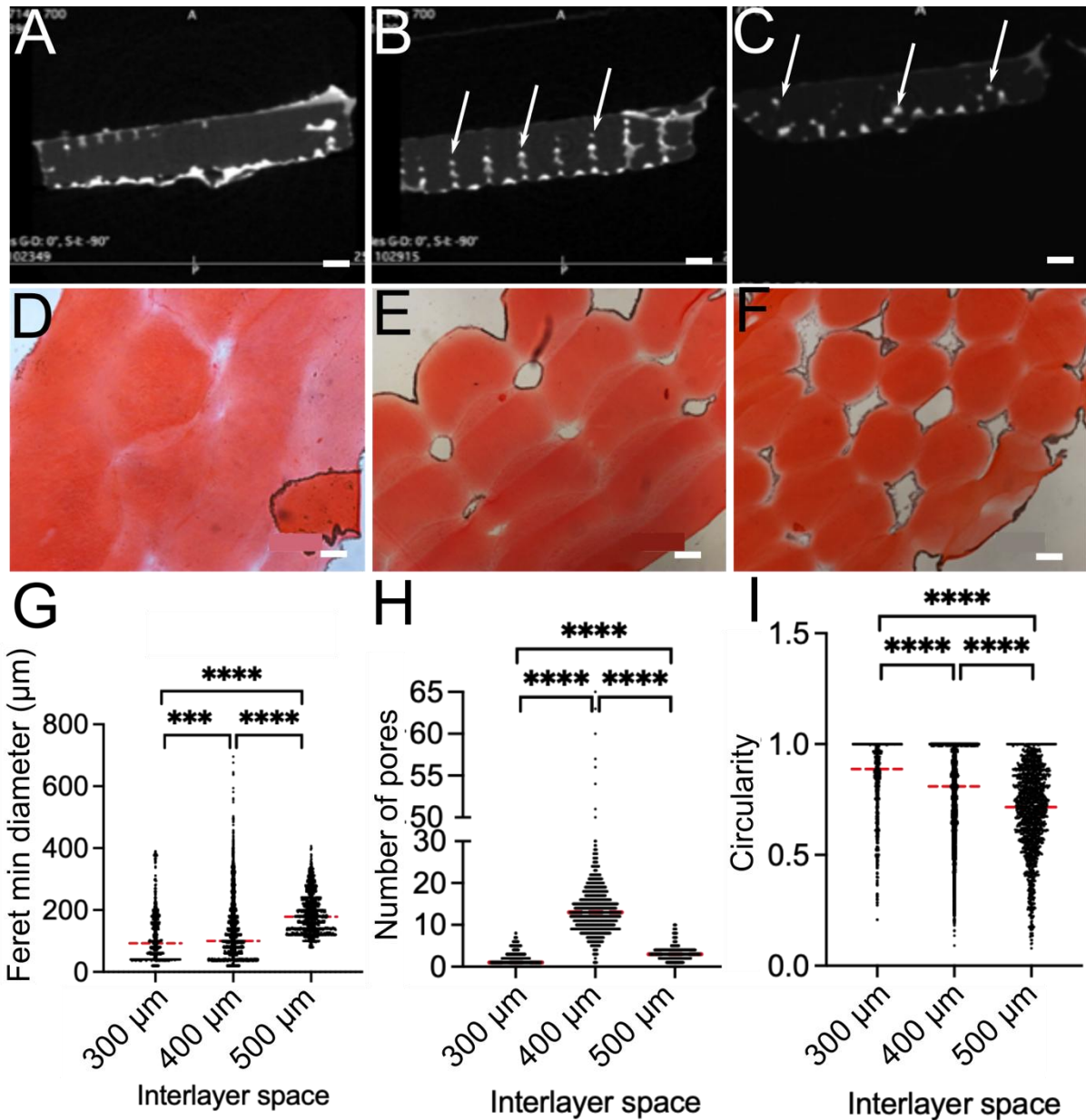


**Figure 2.** Intrinsic porosity of 3D-printed collagen hydrogels, a stack of layers made of 330  $\mu\text{m}$  thick filaments. The top layer is cohesive with the previous ones, generating an inherent porosity. (A-C) Transverse sections of 3D-printed hydrogels observed by micro-CT (scale bar 1 mm). The white arrows indicate pores (filled with contrast agent). Interlayer space: (A) 300  $\mu\text{m}$ , (B) 400  $\mu\text{m}$ , and (C) 500  $\mu\text{m}$ . (D-F) Sirius red staining on histological sections from printed collagen hydrogels (scale bar 100  $\mu\text{m}$ ). Interlayer space: (D) 300  $\mu\text{m}$ , (E) 400  $\mu\text{m}$  and (F) 500  $\mu\text{m}$ . (G) Image analysis using Image J of pore size distribution depending on the interlayer space (Feret min diameter of pores – the largest circle that enters the pore). (H) Number of pores observed thanks to the analysis (I) Image analysis of pores circularity (Red lines indicate the median, \*\*\*\*:  $p < 0.0001$ , Kruskal-Wallis test). (n=3 for each condition).

### 3.2. Evaluation of collagen anisotropy

Different techniques were used to assess collagen anisotropy from a macroscopic aspect (second-harmonic generation (SHG) and polarized-light microscopies (PLM)) to a microscopic aspect with cell alignment along collagen fibers. First, printed hydrogels exhibited different SHG signal intensities according to the gelling method for the same quantity of collagen (see Table 1). Printed collagen constructs gelled with ammonia vapors alone (1 day  $\text{NH}_3$ ) or combined with PBS 5X for 30 min (30 min PBS/1 day 1 day  $\text{NH}_3$ ) exhibited a weak SHG intensity compared to other constructs (Figure 3 – row A), showing the disorganization of collagen fibrils. The analysis under crossed-polarized light microscopy confirmed the results obtained by SHG (Figure 3 – row B). Collagen birefringence was visible for all the conditions gelled in PBS 5X for at least one day.

Conversely, casted hydrogels did not exhibit collagen birefringence regardless of the gelling process (Figure 3 - last column and Figure S3). Last, the presence of anisotropy was investigated by the culture of fibroblasts at the hydrogel surface. After 24 hours in culture, fibroblasts aligned along the axis of the filaments of 3D-printed hydrogels (Figure 3 – row C). The graphs obtained with the Orientation J plug-in (Fiji) demonstrated that all printed conditions, except 1 day  $\text{NH}_3$  and 30 min PBS/1 day  $\text{NH}_3$ , were suitable for fibroblast alignment (Figure 3 – row D). In contrast, fibroblasts were randomly oriented when seeded onto casted hydrogels (Figure 3 - last column and Figure S3). Hence, a minimum of 24 hours in PBS 5X was required to maintain the anisotropy created by the printing process.

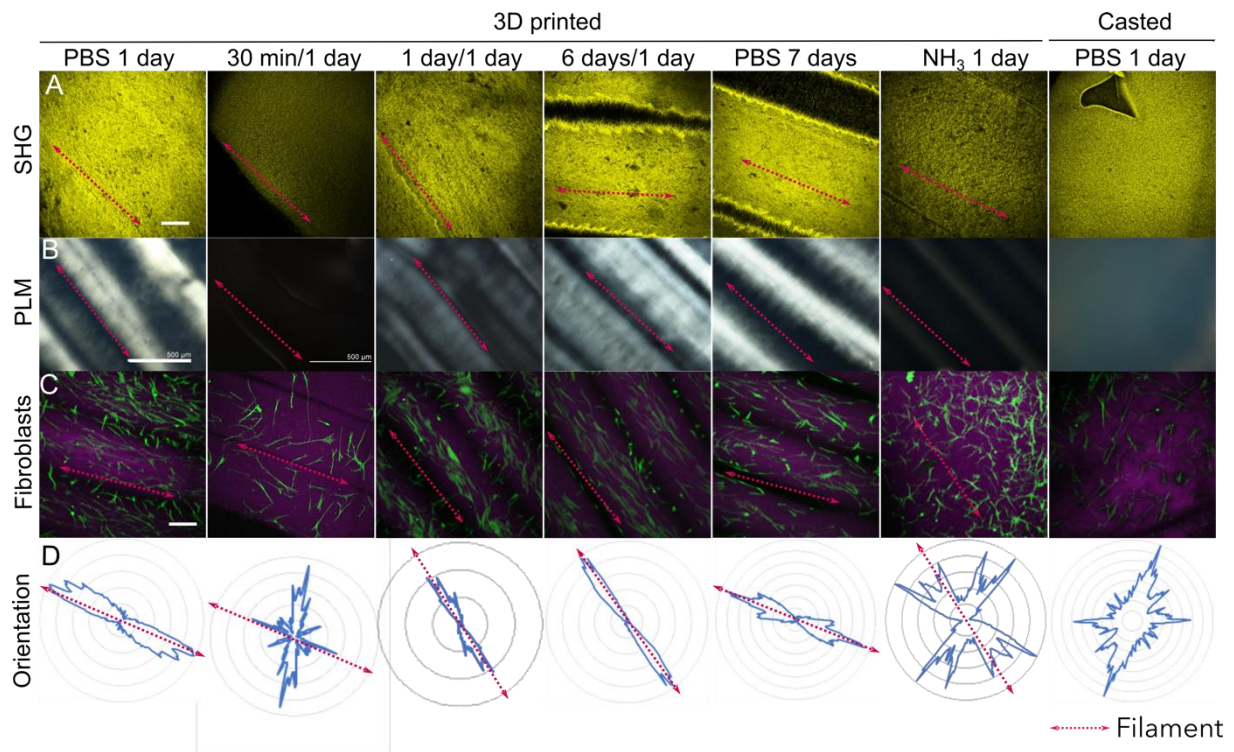


**Figure 3.** Anisotropy observation and quantification within 3D-printed dense collagen hydrogels. (A) Second-harmonic Microscopy (SHG) Imaging (scale bar 100  $\mu\text{m}$ ). (B) Polarized Light microscopy (PLM) (scale bar 500  $\mu\text{m}$ ). (C) Fibroblasts alignment on hydrogels. Green: Fibroblasts labeled with Alexa Fluor 488 Phalloidin, Purple: SHG signal from collagen fibrils. (scale bar 250  $\mu\text{m}$ ). (D) Quantification of cell alignment by Orientation J treatment. Percentage of cells depending on the angle they made with the filament orientation ( $0^\circ$ ). The pink arrow indicates the filament orientation.  $n=6$  for each experiment.

### 3.3. Impact of 3D printing on collagen mechanical properties

To monitor the impact of the gelling process on mechanical properties, rheology was first performed on the different casted hydrogels. 1 day of  $\text{NH}_3$  gelling led to the formation of hydrogels with a high storage modulus,  $G'$  around 2.5 kPa. The combination of gelling methods 1 day PBS/ 1 day  $\text{NH}_3$  generated hydrogels with a similar storage modulus. Hydrogels only gelled with PBS 5X (1 day PBS, 7 days PBS) exhibited a lower stiffness with  $G'$  around 1 kPa. The other conditions combining PBS 5X and  $\text{NH}_3$ , *i.e.*, 30 min PBS/1 day  $\text{NH}_3$  and 6 days PBS/1 day  $\text{NH}_3$ , did not permit the generation of hydrogels with high mechanical properties (Figure 4-A). Rheology was suitable for casted isotropic gels but was inadequate for printed gels due to their anisotropy. Thus, tensile tests were performed on

printed hydrogels (along fiber direction (//) and perpendicular ( $\perp$ ) to fiber direction) to observe the impact of printing and anisotropy on the mechanical response. For 1 day PBS constructs, a strong mismatch of the mechanical responses are observed when stretching the sample along or perpendicularly to the fibers axis. These differences in mechanical behavior evidence a strong anisotropy at macroscopic scale, *i.e.*, sample scale. The extreme softness of the mechanical response under perpendicular conditions suggests a predominant strain response arising from weak interfaces between filaments. (Figure 4-B). A 1 day PBS/1 day  $\text{NH}_3$  gelling reproduced qualitatively the same behavior, *i.e.*, with a significant different mechanical responses between the traction along the fibrils and perpendicularly (Figure 4-C). However, the difference was lower. Last, for 1 day  $\text{NH}_3$  constructs, the curves were very close, showing no significant differences between the two orientations of stretching. This evidences the absence of macroscopic anisotropy (Figure 4-D). The Young's modulus obtained by a linear fit on the first 5 % strain did not reveal significant differences between 1 day PBS and 1 day PBS/1 day  $\text{NH}_3$  constructs (Figure S4).

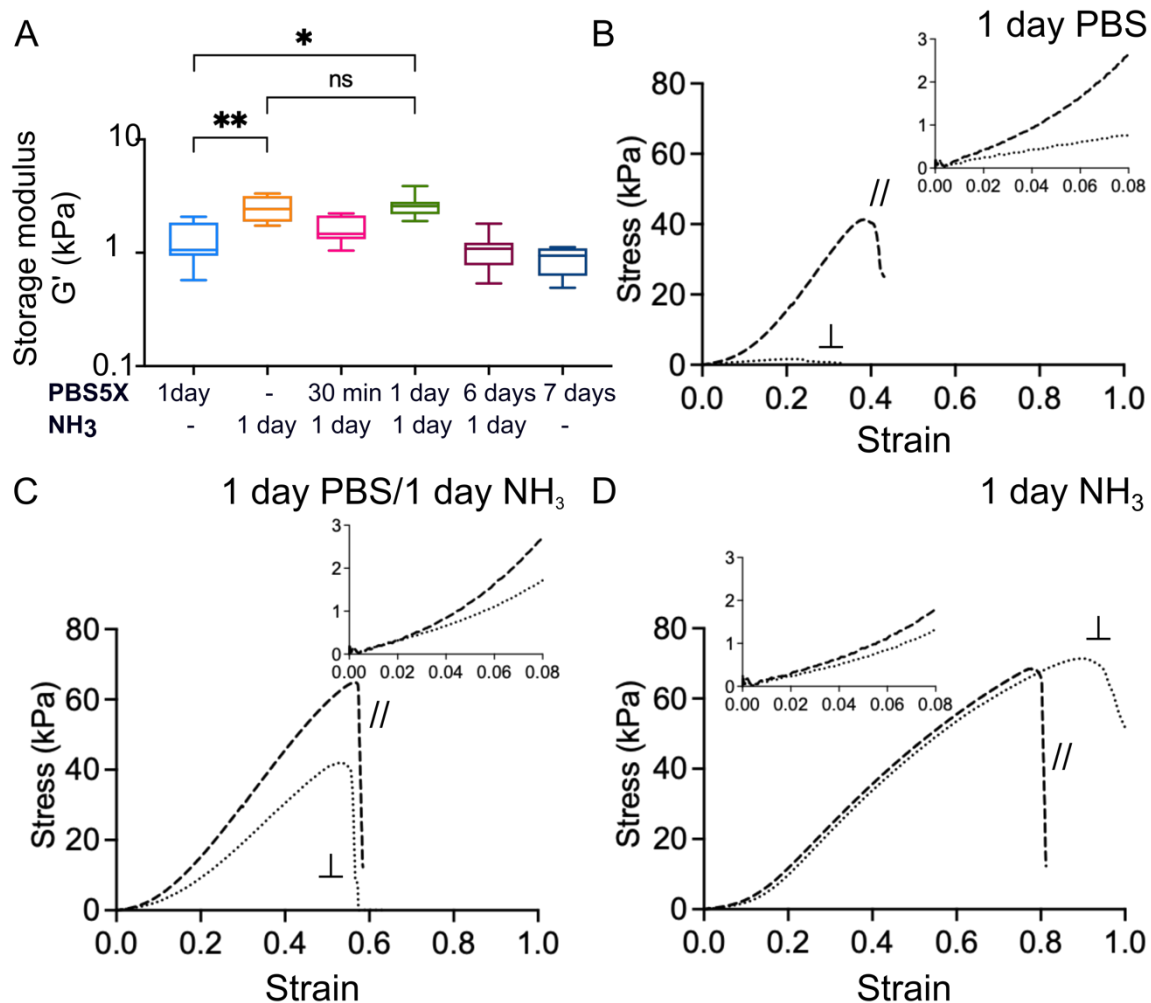


**Figure 4.** (A) Storage Modulus ( $G'$ ) of dense collagen hydrogels assessed by rheological measurements. (\*\*\*:  $p < 0.001$ , \*\*:  $p < 0.01$ , ns:  $p > 0.05$ , Kruskal-Wallis test). (B-D) Tensile test curves of printed collagen construct stretched along the fibril direction (//) (non-continuous line) and perpendicular ( $\perp$ ) to the fibril direction (dotted line). Experiments were performed for (B) 1 day PBS, (C) 1 day PBS/1 day NH<sub>3</sub>, and (D) 1 day NH<sub>3</sub>. (n=3 for each condition)

### 3.4. Fibrillar structure of collagen hydrogels

Collagen fibrillar structure was analyzed by Transmission Electron Microscopy (TEM) to observe the impact of the printing process and gelling conditions on fibrillogenesis. Using ImageJ, a surface density of fibrils was measured on TEM images to compare fibrillogenesis in printed and casted hydrogels. This analysis showed that the fibril density measured in printed gels formed with PBS (1 day PBS or 7 days PBS) or with mixed conditions (30 min PBS/1 day NH<sub>3</sub>, 1 day PBS/1 day NH<sub>3</sub>, 6 days PBS/1 day NH<sub>3</sub>) was higher than that in casted hydrogels (Figure 5-A, B and C). This increase in fibril density was not visible for 1 day of



NH<sub>3</sub> gelling condition. The differential calorimetry experiment did not demonstrate any modifications in the temperature of the denaturation peak of collagen, whatever the gelling condition. Thus, all conditions formed mature collagen fibrils (Figure 5-D).

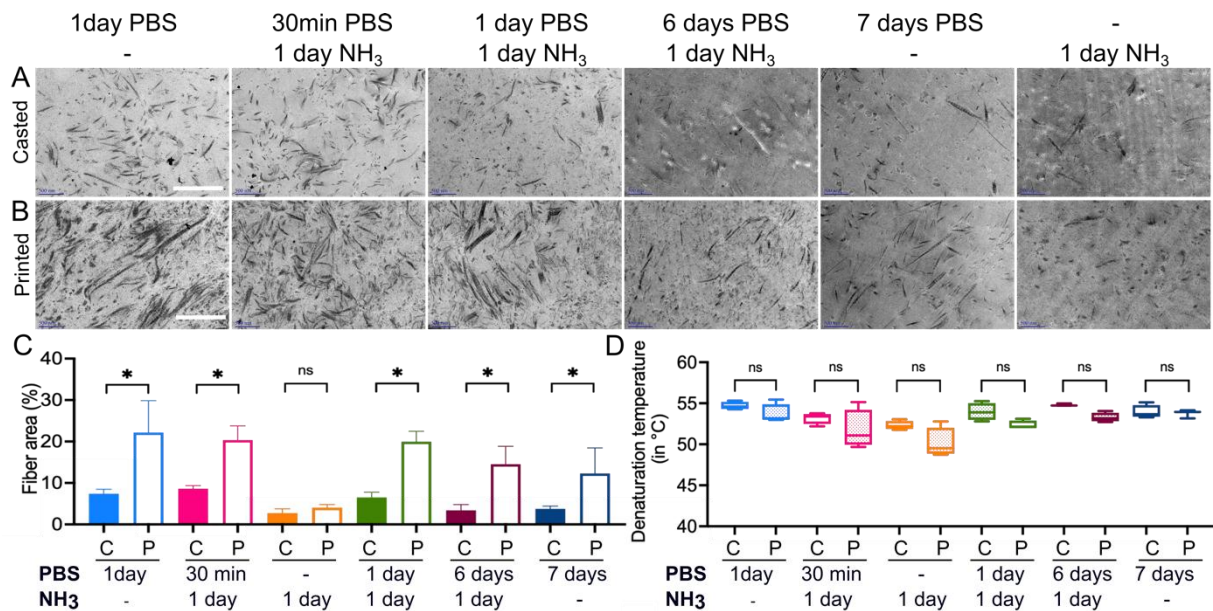


**Figure 5.** Collagen fibrillogenesis according to the gelling conditions observed by Transmission Electron Microscopy. (A) images of casted hydrogels (scale bar 500 nm). (B) 3D-printed hydrogels (scale bar 500 nm). (C) Analysis of the area covered by fibrils in casted - C - and printed - P - gels. (D) Denaturation temperature of collagen fibrils within casted - C - or 3D-printed - P - hydrogels regarding the gelling process. (n=3 for each condition, \*: p < 0.05, Mann-Whitney test).

### 3.5. Addition of large channels within the collagen scaffold for cell colonization

*In vivo*, muscle bundles are more significant than the 100 μm created by the stacking of filaments. Hence, an additional porosity is required for cell cultivation. The best combination between anisotropy and mechanical properties was 1 day PBS/1 day NH<sub>3</sub> and was selected for the rest of the study. To have reproducible hydrogels, a dedicated plastic mold was created to place the needles in the same position (Figure 6-A). Collagen constructs were directly printed inside this mold. After a 30 min period post-printing in PBS 5X, forming gels were perforated with 600 μm needles using the dedicated holes. Then, the gelling was extended with 1 day PBS/1 day NH<sub>3</sub> to increase mechanical properties. After complete gelling, micro Computed Tomography revealed 2 well-defined straight channels inside the printed hydrogels (Figure 6-

B). The smaller intrinsic pores obtained by the printing process were also visible on the scan. Collagen birefringence was still visible. The SHG signal was also not altered (Figure 6-C et D), indicating that the addition of needles post-printing did not disturb the anisotropy generated during the first short gelling period in PBS 5X (Figure S5).

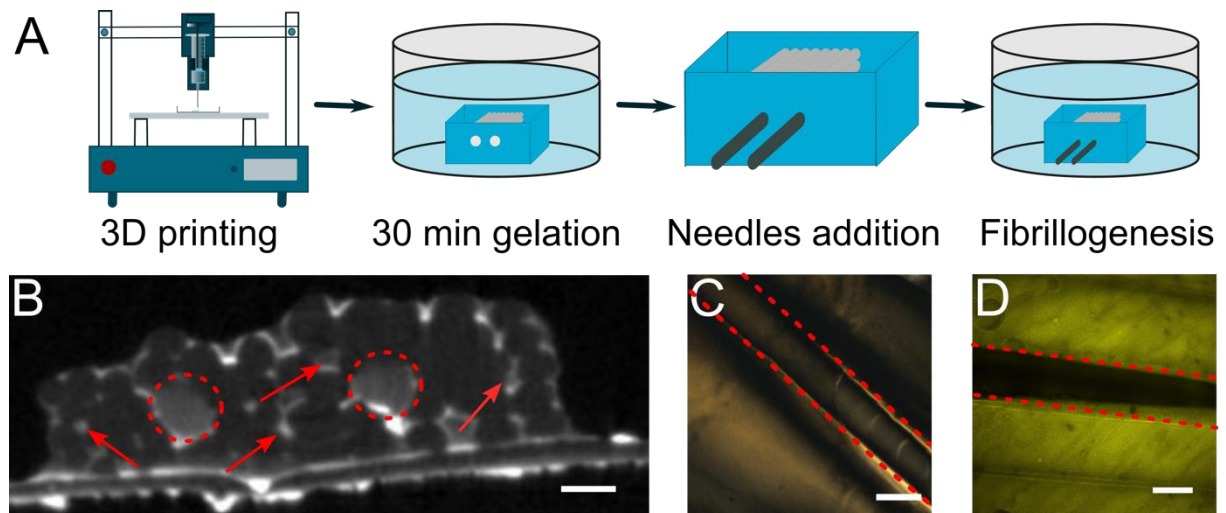


**Figure 6.** Generation of large channels within printed hydrogels without alteration of collagen anisotropy. (A) Set up: needles molding during collagen gelation. (B) Micro Computed Tomography of a 3D-printed gel with 2 needles. Two networks of pores were observed: one around 100  $\mu\text{m}$  thanks to printing (intrinsic porosity – red arrows) and the other at 600  $\mu\text{m}$  (needles – red circles) (scale bar 500  $\mu\text{m}$ ). (C) Cross-polarized light microscopy of sections of printed hydrogel (1 day PBS/1 day  $\text{NH}_3$ ) with the presence of needles. (scale bar 500  $\mu\text{m}$ ). (D) Second-harmonic generation imaging of sections of printed gel with needles (scale bar 250  $\mu\text{m}$ ).

### 3.6. Murine skeletal myoblast colonization and differentiation inside large channels

Myoblasts were seeded inside the large channels created within the perimysium-like scaffold to model muscle fibers. Muscle fibers are composed of myoblasts surrounded by loose connective tissue made of collagen IV and laminin. The use of Matrigel® reproduced the latter. C2C12 murine skeletal myoblasts were seeded and cultured for 4 or 7 days. Regardless of the medium used, proliferation, or differentiation, myoblasts aligned along the axis of the pores and filled the channel. When cultured in a differentiation medium, some parallel, multinucleated densely-packed myotubes expressing heavy myosin chains (MF20) could be observed on day 4, reproducing a muscular bundle. Fused myoblasts forming myotubes were

easily visible with phalloidin staining thanks to their enlarged shape and numerous nuclei (Figure 7). Seven days in the differentiation medium did not show significant changes in differentiation (Figure S6).

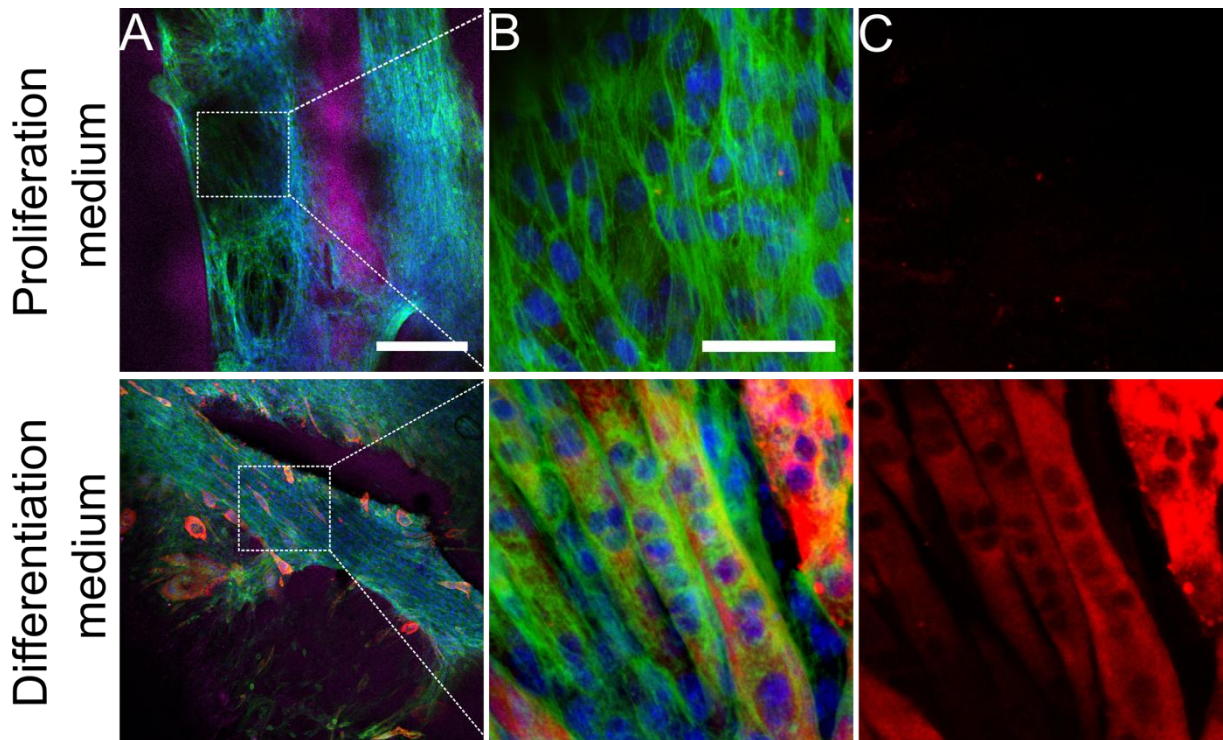


**Figure 7.** C2C12 colonization and differentiation into myotubes within the large pores generated by needles (600  $\mu\text{m}$ ). (A) Longitudinal view of pores (scale bar 100  $\mu\text{m}$ ). Green: actin, blue: nucleus, red: MF20. (B) Zoom on myotubes alignment and (C) myosin staining (scale bar 50  $\mu\text{m}$ ) (n=6 for each condition)

#### 4. Discussion

This study aimed to design a novel *in vitro* 3D model of skeletal muscle combining a physiologically relevant artificial matrix with muscle bundles. A scaffold in the form of a dense collagen hydrogel was synthesized to mimic the fascia. This synthetic matrix had to mimic the four main characteristics of the native one, *i.e.*, its biochemical composition, stiffness, porosity, and anisotropy. Then, this scaffold was cellularized with C2C12 myoblasts embedded inside Matrigel® to reproduce the muscle bundles (myotubes + endomysium). After *in situ* differentiation, cells assembled into mature multinucleated myotubes.



First, the muscle fascia comprises collagen I and III, proteoglycans, and glycosaminoglycans [37]. The fibril-forming collagen I is a building block of great interest in fabricating the scaffold. This protein is known to strengthen connective tissues and is the natural support for cell adhesion. Unfortunately, collagen-based hydrogels are currently manufactured from low concentrated solutions ( $<4 \text{ mg}\cdot\text{mL}^{-1}$ ), possess poor mechanical properties, and shrink under cellular contractile activities [13,38]. These drawbacks can be circumvented without any crosslinking by increasing the collagen concentration. This study used evaporation to obtain a printable collagen solution at  $30 \text{ mg}\cdot\text{mL}^{-1}$  [39], mimicking the physiological concentration observed in muscle ECM [11]. Despite the high viscosity of concentrated solutions, their printing at  $2 \text{ mm}\cdot\text{s}^{-1}$  was suitable taking advantage of the shear-thinning behavior of collagen I [19,31]. Parameters of extrusion are consistent with the study of Rhee and co-workers showing that a collagen concentration superior to  $17 \text{ mg}\cdot\text{mL}^{-1}$  is required to obtain printing accuracy and shape fidelity [23]. Unfortunately, without printing bath, the round shape of these extruded filaments rapidly disappeared in contact with air and the other filaments. Based on Picaut and co-workers' study, a printing bath made of PBS 5X enabled good shape fidelity and rapid gelling [19]. The diameter of extruded threads remained stable ( $330 \mu\text{m}$ ) without swelling or shrinkage, thanks to the appropriate ionic strength. In addition, thanks to the interlayer space used, a cohesive and well-organized structure were generated.

The muscular perimysium topography relies on collagen anisotropy. In these tissues, fibrils are highly oriented in the same direction to promote mechanotransduction inside the skeletal muscle [37]. In our study, the extrusion process creates an intrinsic anisotropy by aligning collagen molecules due to the shearing stress the needle applied to the collagen. This alignment is maintained by the PBS 5X bath, which rapidly diffuses (in a minute) within the whole volume of the thin collagen filaments and neutralizes acetic acid. Interestingly, intrinsic anisotropy is also maintained at the scale of in dense hydrogels thanks to collagen fibrils

alignment forming in place of collagen triple helices. Picaut demonstrated that a concentration superior to  $30 \text{ mg}\cdot\text{mL}^{-1}$  within a printing bath containing PBS 5X permitted to obtain isolated anisotropic threads. However, 3D cohesive and complex constructs made of anisotropic and dense filaments of pure collagen I with a controlled concentration had not been described yet. Collagen anisotropy of 3D cohesive constructs is often obtained after printing composite materials consisting of decellularized cornea matrix, collagen/Pluronic 127, or a collagen/hyaluronic acid to ensure a mechanical strength [40–42]. The major drawbacks of these systems are the absence of biomimetic collagen fibrils, the significant volume loss after polymer removal, or the strong collagen interaction with the other polymers, thereby preventing an adequate interaction scaffold/cells. In this study, pure dense collagen was very close to the physiological ECM structure and promoted muscle bundles-perimysium interactions.

After printing, an extended gelling time was required to obtain a complete collagen fibrillogenesis and suitable mechanical properties. During collagen gelling, two phenomena compete: collagen lateral self-assembling into fibrils (fibrillogenesis) and forming physical crosslinking nodes between collagen molecules to get a hydrogel [35,43]. Fibrillogenesis is strongly impacted by collagen concentration, ionic strength, and pH [44]. In this work, two methods were used for the extended gelling: (1) gelling with PBS 5X (pH 7.4, high ionic strength) and (2)  $\text{NH}_3$  vapors (pH 11, low ionic strength). PBS gelling starts immediately, but fibrils length and thickness evolve across time, whereas  $\text{NH}_3$  vapors trigger a rapid gelling after a lag phase (time for  $\text{NH}_3$  to dissolve and diffuse into the collagen solution). The high ionic strength promotes fibril growth, which explains the larger diameter of fibrils observed in PBS 5X compared to  $\text{NH}_3$ . [35]. However, fibrillogenesis occurred efficiently in all conditions as a denaturation peak at  $55 \text{ }^\circ\text{C}$  was always observed [45].

The pH highly impacts collagen hydrogel mechanical properties during the gelling method [44]. At pH 10-11, collagen molecules are negatively charged, and electrostatic interactions are favored to form physical crosslinking junctions, but hydrophobic interactions required for collagen fibrillogenesis are inhibited. This explains the high mechanical properties and the low fibril diameter observed in hydrogels only gelled with  $\text{NH}_3$  [35,39]. On the contrary, PBS gelling favors fibril growth but not physical crosslinking, leading to lower mechanical properties.

The traction tests performed along with the fibril orientation and perpendicularly to this orientation revealed different mechanical behaviors for the 1 day PBS and 1 day PBS/1 day  $\text{NH}_3$  constructs. Unlike hydrogels formed with  $\text{NH}_3$ , the tensile test curves demonstrated the anisotropy at the macroscopic scale of these constructs as the tensile curves differ according to the stretching axis, impacting Young's modulus.

The condition leading to a biomimetic muscle ECM mimicking perimysium was 1 day PBS/1 day  $\text{NH}_3$  because it combines the fibril formation and alignment and the appropriate mechanical properties. When 1 day PBS/1 day  $\text{NH}_3$  printed constructs were stretched in the fibril direction, Young's modulus of hydrogels gelled increased up to  $25.1 \pm 9.6$  kPa but slightly decreased down to  $16.01 \pm 7.6$  kPa when extended perpendicularly (Figure S4). All these values remain in the range of stiffness (8 – 25 kPa), promoting myogenic differentiation [46]. In addition, the mechanical behavior is elastic when a 10 % deformation is applied, as seen on traction curves. For the first time, by combining two methods of collagen gelling (PBS 5X and  $\text{NH}_3$ ), we obtained anisotropic collagen constructs made of large biomimetic fibrils exhibiting the mechanical behavior of the muscle ECM [47].

An anisotropic dense collagen hydrogel is not sufficient to mimic muscle extracellular matrix. Anisotropic porosity is significant since around 300 capillaries per  $\text{mm}^2$  are necessary to meet the oxygen and nutrient demands [48]. *In vivo*, muscle cells form muscle bundles from mm to

cm long [49]. These muscle fibers are surrounded by the perimysium, in which a dense capillary network brings oxygen and nutrients to the cells [12]. *In vitro*, diffusion is insufficient to ensure nutrients and oxygen diffusion into a compact 3D dense collagen construct. The 3D printing process of our study created an adequate intrinsic porosity between the different collagen layers. Thanks to the high shape fidelity, extruded threads remain round and will gently be superposed on top of each other. During the initial gelling, the filaments partially fused with their neighbors to allow the construct cohesiveness. From a side view, the construct resembles a “stack of wood” with interstitial space between every filament. This one-step process generates a porosity of 100  $\mu\text{m}$  in diameter cylindrical pores crossing the anisotropic construct and is suitable for nutrients and oxygen diffusion.

Meanwhile, in this condition, the cohesiveness of the construct was preserved. This porosity generation does not require additional steps such as heating compared to sacrificial ink techniques or porogen leaching. Long term stability was experienced in aqueous conditions at neutral pH, collagen gel constructs can be stored for several months without degradation. Unlike the bidirectional methods currently used in 3D printing (angle between one layer and the upper one  $90^\circ$ ) to improve the construct cohesiveness, the straight channels generated by our procedure allowed for a rapid and effective liquid diffusion. [31].

This intrinsic porosity is adequate for nutrient diffusion but is too tiny for muscle cell colonization and organization. A muscle bundle comprises 20 to 60 muscle cells (20-100  $\mu\text{m}$  in diameter) corresponding to a final diameter of 400 to 6000  $\mu\text{m}$  [1]. A 600  $\mu\text{m}$  diameter corresponds to the physiological range of a muscle bundle. Generating large channels by 3D printing is difficult without using sacrificial ink as channels tend to collapse [50]. For this reason, we used a molding method. Two straight channels were easily created using 600  $\mu\text{m}$  needles within dense collagen hydrogels without disturbing the collagen alignment after removal. Hence, Anisotropy appeared at two different scales: anisotropic channels (high

length/width ratio), forcing myoblasts to align [34,51], and inherent anisotropy within channel walls (aligned fibrils of collagen due to the printing process).

C2C12 myoblasts were seeded into the large pores of printed hydrogels using the 1 day PBS/1 day NH<sub>3</sub> gelling condition to observe myotubes formation in a 3D biomimetic environment. Matrigel® mimicked the endomysium because of its similar composition, mostly collagen IV and laminins [37]. After 4 days of differentiation, large, densely-packed, and aligned multinucleated myotubes expressing myosin heavy chain were observed within the whole volume of channels. Hence, the scaffold was suitable to sustain the development of fused myoblasts into myotubes in 3D after 4 days. Previous works investigated the C2C12 behavior on different porous collagen structures [29,34]. Unfortunately, the 3D organization of cells in these materials was questionable because cells only adhered to the pore surface and did not fill up the entire volume to acquire an organotypic organization.

The model of skeletal muscle presented here is based on developing a biomimetic ECM. Despite interesting cell contractility results, 2D muscle models do not study the cell-ECM interactions and lack 3D organotypic structure. 3D models seemed to bring a new approach, but the extracellular matrix role was often neglected. The most widespread 3D *in vitro* model was developed to study contractility. A low-concentrated collagen solution encapsulates cells in a 3D shape before creating a microtissue between PDMS pillars [7,8]. However, cells shrank the hydrogel and died because of a lack of nutrients and oxygen diffusion [52]. In addition, ECM physical properties are poorly tunable and controllable due to shrinkage. Another model used synthetic polymers to create large channels for myoblasts seeding [51,53]. This scaffold had high mechanical properties but failed to reproduce cell adhesion cues. Other approaches are based on the 3D printing of a cell-laden ink to create cellularized threads mimicking muscular bundles [24,25], but collagen is rarely used. Kim and co-workers developed bioprinted threads of dense collagen colonized by C2C12, but the diameter of their

muscle bundle is at least twice lower compared to physiological bundles [20]. The poor nutrient diffusion inside dense collagen justifies this choice.

In contrast, in our model the biochemical cues are restored thanks to collagen I and Matrigel®. Our collagen constructs' stiffness, porosity, and anisotropy imitate the muscle cell microenvironment.

## **5. Conclusions**

In this study, we have designed a biomimetic hydrogel possessing the physical properties of the muscle ECM and colonized it with C2C12 myoblasts to form muscle bundles. The unidirectional 3D printing of dense collagen solutions within an appropriate gelling bath is an adequate strategy to mimic the muscle extracellular matrix. This single-step technique produces dense anisotropic hydrogels possessing interesting mechanical properties and a controlled anisotropic porosity suitable for nutrient and O<sub>2</sub> diffusion. In addition, larger channels dedicated to cell colonization and muscle bundle organization can be easily set by molding without disturbing the hydrogel topography and mechanical properties. Last, this model allows the muscle cell alignment within channels filled with Matrigel® and their differentiation into myotubes, thereby reproducing the structure of a skeletal muscle bundle. Compared to 2D models, this 3D novel model brings more complexity despite its simple fabrication. It will permit to study of the impact of the muscle ECM properties on cell phenotype and contraction.

## **Acknowledgements**

The authors thank PhD. Lotfi Slimani for micro-computed tomography imaging from the Life Imaging Facility of Paris University supported by France Live Imaging (grant ANR 11-INBS-

0006) and Infrastructures Santé. We also thank Gervaise Mosser for her help in transmission electron microscopy.

## Fundings

This research was funded by Sorbonne Université, CNRS, INSERM and the AFM-Téléthon (contract number: 22142).

## Supporting Information

Supporting Information is available from XX

## Declaration of competing interests

The authors declare no conflict of interests relevant to this work.

## References

1. Slutsky, D.J. Electrodiagnostic Testing of the Upper Extremity. In *Peripheral Nerve Surgery*; Elsevier, 2006; pp. 319–355 ISBN 978-0-443-06667-2.
2. McLoon, L.K.; Vicente, A.; Fitzpatrick, K.R.; Lindström, M.; Pedrosa Domellöf, F. Composition, Architecture, and Functional Implications of the Connective Tissue Network of the Extraocular Muscles. *Investig. Ophthalmology Vis. Sci.* **2018**, *59*, 322, doi:10.1167/iovs.17-23003.
3. Csapo, R.; Gumpenberger, M.; Wessner, B. Skeletal Muscle Extracellular Matrix – What Do We Know About Its Composition, Regulation, and Physiological Roles? A Narrative Review. *Front. Physiol.* **2020**, *11*, 253, doi:10.3389/fphys.2020.00253.
4. Choi, I.Y.; Lim, H.; Estrellas, K.; Mula, J.; Cohen, T.V.; Zhang, Y.; Donnelly, C.J.; Richard, J.-P.; Kim, Y.J.; Kim, H.; et al. Concordant but Varied Phenotypes among Duchenne Muscular Dystrophy Patient-Specific Myoblasts Derived Using a Human iPSC-Based Model. *Cell Rep.* **2016**, *15*, 2301–2312, doi:10.1016/j.celrep.2016.05.016.
5. Kim, J.J.; Hou, L.; Huang, N.F. Vascularization of Three-Dimensional Engineered Tissues for Regenerative Medicine Applications. *Acta Biomater.* **2016**, *41*, 17–26, doi:10.1016/j.actbio.2016.06.001.
6. Young, C.S.; Hicks, M.R.; Ermolova, N.V.; Nakano, H.; Jan, M.; Younesi, S.; Karumbayaram, S.; Kumagai-Cresse, C.; Wang, D.; Zack, J.A.; et al. A Single CRISPR-Cas9 Deletion Strategy That Targets the Majority of DMD Patients Restores Dystrophin Function in HiPSC-Derived Muscle Cells. *Cell Stem Cell* **2016**, *18*, 533–540, doi:10.1016/j.stem.2016.01.021.
7. Agrawal, G.; Aung, A.; Varghese, S. Skeletal Muscle-on-a-Chip: An in Vitro Model to Evaluate Tissue Formation and Injury. *Lab. Chip* **2017**, *17*, 3447–3461,

doi:10.1039/C7LC00512A.

8. Maffioletti, S.M.; Sarcar, S.; Henderson, A.B.H.; Mannhardt, I.; Pinton, L.; Moyle, L.A.; Steele-Stallard, H.; Cappellari, O.; Wells, K.E.; Ferrari, G.; et al. Three-Dimensional Human iPSC-Derived Artificial Skeletal Muscles Model Muscular Dystrophies and Enable Multilineage Tissue Engineering. *Cell Rep.* **2018**, *23*, 899–908, doi:10.1016/j.celrep.2018.03.091.
9. Sharples, A.P.; Player, D.J.; Martin, N.R.W.; Mudera, V.; Stewart, C.E.; Lewis, M.P. Modelling *in Vivo* Skeletal Muscle Ageing *in Vitro* Using Three-Dimensional Bioengineered Constructs: 3D Bioengineered Model of Aged Skeletal Muscle. *Aging Cell* **2012**, *11*, 986–995, doi:10.1111/j.1474-9726.2012.00869.x.
10. Camman, M.; Joanne, P.; Agbulut, O.; Hélarly, C. 3D Models of Dilated Cardiomyopathy: Shaping the Chemical, Physical and Topographical Properties of Biomaterials to Mimic the Cardiac Extracellular Matrix. *Bioact. Mater.* **2021**, S2452199X21002607, doi:10.1016/j.bioactmat.2021.05.040.
11. Wilson, L.K. Characterization of Human Muscle Extracellular Matrix. **2015**, 64.
12. Carmeliet, P.; Jain, R.K. Angiogenesis in Cancer and Other Diseases. **2000**, *407*, 9.
13. Chieh, H.-F.; Sun, Y.; Liao, J.-D.; Su, F.-C.; Zhao, C.; Amadio, P.C.; An, K.-N. Effects of Cell Concentration and Collagen Concentration on Contraction Kinetics and Mechanical Properties in a Bone Marrow Stromal Cell-Collagen Construct. *J. Biomed. Mater. Res. A* **2009**, 9999A, NA-NA, doi:10.1002/jbm.a.32606.
14. Chen, S.; Hirota, N.; Okuda, M.; Takeguchi, M.; Kobayashi, H.; Hanagata, N.; Ikoma, T. Microstructures and Rheological Properties of Tilapia Fish-Scale Collagen Hydrogels with Aligned Fibrils Fabricated under Magnetic Fields. *Acta Biomater.* **2011**, *7*, 644–652, doi:10.1016/j.actbio.2010.09.014.
15. Joanne, P.; Kitsara, M.; Boitard, S.-E.; Naemetalla, H.; Vanneaux, V.; Pernot, M.; Larghero, J.; Forest, P.; Chen, Y.; Menasché, P.; et al. Nanofibrous Clinical-Grade Collagen Scaffolds Seeded with Human Cardiomyocytes Induces Cardiac Remodeling in Dilated Cardiomyopathy. *Biomaterials* **2016**, *80*, 157–168, doi:10.1016/j.biomaterials.2015.11.035.
16. Matthews, J.A.; Wnek, G.E.; Simpson, D.G.; Bowlin, G.L. Electrospinning of Collagen Nanofibers. *Biomacromolecules* **2002**, *3*, 232–238, doi:10.1021/bm015533u.
17. Torbet, J.; Malbouyres, M.; Builles, N.; Justin, V.; Roulet, M.; Damour, O.; Oldberg, Å.; Ruggiero, F.; Hulmes, D.J.S. Orthogonal Scaffold of Magnetically Aligned Collagen Lamellae for Corneal Stroma Reconstruction. *Biomaterials* **2007**, *28*, 4268–4276, doi:10.1016/j.biomaterials.2007.05.024.
18. Kitsara, M. Fabrication of Cardiac Patch by Using Electrospun Collagen Fibers. *Microelectron. Eng.* **2015**, 5.
19. Picaut, L.; Trichet, L.; Ronsin, O.; Haye, B.; Génois, I.; Baumberger, T.; Mosser, G. Pure Dense Collagen Threads from Extrusion to Fibrillogenesis Stability. *Biomed. Phys. Eng. Express* **2018**, *4*, 035008, doi:10.1088/2057-1976/aaab78.
20. Kim, W.; Kim, G. A Functional Bioink and Its Application in Myoblast Alignment and Differentiation. *Chem. Eng. J.* **2019**, *366*, 150–162, doi:10.1016/j.cej.2019.02.071.
21. Griffanti, G.; Rezabeigi, E.; Li, J.; Murshed, M.; Nazhat, S.N. Rapid Biofabrication of Printable Dense Collagen Bioinks of Tunable Properties. *Adv. Funct. Mater.* **2020**, *30*, 1903874, doi:10.1002/adfm.201903874.
22. Kim, J.H.; Seol, Y.-J.; Ko, I.K.; Kang, H.-W.; Lee, Y.K.; Yoo, J.J.; Atala, A.; Lee, S.J. 3D Bioprinted Human Skeletal Muscle Constructs for Muscle Function Restoration. *Sci. Rep.* **2018**, *8*, 12307, doi:10.1038/s41598-018-29968-5.
23. Rhee, S.; Puetzer, J.L.; Mason, B.N.; Reinhart-King, C.A.; Bonassar, L.J. 3D Bioprinting of Spatially Heterogeneous Collagen Constructs for Cartilage Tissue Engineering. *ACS Biomater. Sci. Eng.* **2016**, *2*, 1800–1805, doi:10.1021/acsbomaterials.6b00288.



24. Fan, T.; Wang, S.; Jiang, Z.; Ji, S.; Cao, W.; Liu, W.; Ji, Y.; Li, Y.; Shyh-Chang, N.; Gu, Q. Controllable Assembly of Skeletal Muscle-like Bundles through 3D Bioprinting. *Biofabrication* **2022**, *14*, 015009, doi:10.1088/1758-5090/ac3aca.
25. Hwangbo, H. Bio-Printing of Aligned GelMa-Based Cell-Laden Structure for Muscle Tissue Regeneration. *Bioact. Mater.* **2022**, *14*.
26. Datta, P.; Ayan, B.; Ozbolat, I.T. Bioprinting for Vascular and Vascularized Tissue Biofabrication. *Acta Biomater.* **2017**, *51*, 1–20, doi:10.1016/j.actbio.2017.01.035.
27. Ganji, Y.; Li, Q.; Quabius, E.S.; Böttner, M.; Selhuber-Unkel, C.; Kasra, M. Cardiomyocyte Behavior on Biodegradable Polyurethane/Gold Nanocomposite Scaffolds under Electrical Stimulation. *Mater. Sci. Eng. C* **2016**, *59*, 10–18, doi:10.1016/j.msec.2015.09.074.
28. Silver, F.H.; Freeman, J.W.; Seehra, G.P. Collagen Self-Assembly and the Development of Tendon Mechanical Properties. *J. Biomech.* **2003**, *36*, 1529–1553, doi:10.1016/S0021-9290(03)00135-0.
29. Gokyer, S.; Yilgor, E.; Yilgor, I.; Berber, E.; Vrana, E.; Orhan, K.; Monsef, Y.A.; Guvener, O.; Zinnuroglu, M.; Oto, C.; et al. 3D Printed Biodegradable Polyurethaneurea Elastomer Recapitulates Skeletal Muscle Structure and Function. *ACS Biomater. Sci. Eng.* **2021**, acsbiomaterials.1c00703, doi:10.1021/acsbiomaterials.1c00703.
30. Matsugaki, A.; Matsuzaka, T.; Murakami, A.; Wang, P.; Nakano, T. 3D Printing of Anisotropic Bone-Mimetic Structure with Controlled Fluid Flow Stimuli for Osteocytes: Flow Orientation Determines the Elongation of Dendrites. *Int. J. Bioprinting* **2020**, *6*, doi:10.18063/ijb.v6i4.293.
31. Nocera, A.D.; Comín, R.; Salvatierra, N.A.; Cid, M.P. Development of 3D Printed Fibrillar Collagen Scaffold for Tissue Engineering. *Biomed. Microdevices* **2018**, *20*, 26, doi:10.1007/s10544-018-0270-z.
32. Chrobak, K.M.; Potter, D.R.; Tien, J. Formation of Perfused, Functional Microvascular Tubes in Vitro. *Microvasc. Res.* **2006**, *71*, 185–196, doi:10.1016/j.mvr.2006.02.005.
33. Mori, N.; Morimoto, Y.; Takeuchi, S. Skin Integrated with Perfusable Vascular Channels on a Chip. *Biomaterials* **2017**, *116*, 48–56, doi:10.1016/j.biomaterials.2016.11.031.
34. Rieu, C.; Parisi, C.; Mosser, G.; Haye, B.; Coradin, T.; Fernandes, F.M.; Trichet, L. Topotactic Fibrillogenesis of Freeze-Cast Microridged Collagen Scaffolds for 3D Cell Culture. *ACS Appl. Mater. Interfaces* **2019**, *11*, 14672–14683, doi:10.1021/acsami.9b03219.
35. Gobeaux, F.; Mosser, G.; Anglo, A.; Panine, P.; Davidson, P.; Giraud-Guille, M.-M.; Belamie, E. Fibrillogenesis in Dense Collagen Solutions: A Physicochemical Study. *J. Mol. Biol.* **2008**, *376*, 1509–1522, doi:10.1016/j.jmb.2007.12.047.
36. Thrivikraman, G.; Jagiełło, A.; Lai, V.K.; Johnson, S.L.; Keating, M.; Nelson, A.; Schultz, B.; Wang, C.M.; Levine, A.J.; Botvinick, E.L.; et al. Cell Contact Guidance via Sensing Anisotropy of Network Mechanical Resistance. *Proc. Natl. Acad. Sci.* **2021**, *118*, e2024942118, doi:10.1073/pnas.2024942118.
37. Chapman, M.A.; Meza, R.; Lieber, R.L. Skeletal Muscle Fibroblasts in Health and Disease. *Differentiation* **2016**, *92*, 108–115, doi:10.1016/j.diff.2016.05.007.
38. Antoine, E.E.; Vlachos, P.P.; Rylander, M.N. Review of Collagen I Hydrogels for Bioengineered Tissue Microenvironments: Characterization of Mechanics, Structure, and Transport. *Tissue Eng. Part B Rev.* **2014**, *20*, 683–696, doi:10.1089/ten.teb.2014.0086.
39. Helary, C.; Abed, A.; Mosser, G.; Louedec, L.; Letourneur, D.; Coradin, T.; Giraud-Guille, M.M.; Meddahi-Pellé, A. Evaluation of Dense Collagen Matrices as Medicated Wound Dressing for the Treatment of Cutaneous Chronic Wounds. *Biomater. Sci.* **2015**, *3*, 373–382, doi:10.1039/C4BM00370E.
40. Kim, H.; Jang, J.; Park, J.; Lee, K.-P.; Lee, S.; Lee, D.-M.; Kim, K.H.; Kim, H.K.;

- Cho, D.-W. Shear-Induced Alignment of Collagen Fibrils Using 3D Cell Printing for Corneal Stroma Tissue Engineering. *Biofabrication* **2019**, *11*, 035017, doi:10.1088/1758-5090/ab1a8b.
41. Moncal, K.K.; Ozbolat, V.; Datta, P.; Heo, D.N.; Ozbolat, I.T. Thermally-Controlled Extrusion-Based Bioprinting of Collagen. *J. Mater. Sci. Mater. Med.* **2019**, *30*, 55, doi:10.1007/s10856-019-6258-2.
42. Schwab, A.; Hélyary, C.; Richards, R.G.; Alini, M.; Eglin, D.; D'Este, M. Tissue Mimetic Hyaluronan Bioink Containing Collagen Fibers with Controlled Orientation Modulating Cell Migration and Alignment. *Mater. Today Bio* **2020**, *7*, 100058, doi:10.1016/j.mtbio.2020.100058.
43. Lama, M.; Raveendranathan, B.; Brun, J.; Fernandes, F.M.; Boissière, C.; Nassif, N.; Marcellan, A. Biomimetic Tough Gels with Weak Bonds Unravel the Role of Collagen from Fibril to Suprafibrillar Self-Assembly. *Macromol. Biosci.* **2021**, *21*, 2000435, doi:10.1002/mabi.202000435.
44. Achilli, M.; Mantovani, D. Tailoring Mechanical Properties of Collagen-Based Scaffolds for Vascular Tissue Engineering: The Effects of PH, Temperature and Ionic Strength on Gelation. *Polymers* **2010**, *2*, 664–680, doi:10.3390/polym2040664.
45. Frayssinet, A.; Petta, D.; Illoul, C.; Haye, B.; Markitantova, A.; Eglin, D.; Mosser, G.; D'Este, M.; Hélyary, C. Extracellular Matrix-Mimetic Composite Hydrogels of Cross-Linked Hyaluronan and Fibrillar Collagen with Tunable Properties and Ultrastructure. *Carbohydr. Polym.* **2020**, *236*, 116042, doi:10.1016/j.carbpol.2020.116042.
46. Jhala, D.; Vasita, R. A Review on Extracellular Matrix Mimicking Strategies for an Artificial Stem Cell Niche. *Polym. Rev.* **2015**, *55*, 561–595, doi:10.1080/15583724.2015.1040552.
47. Herzog, W.; Powers, K.; Johnston, K.; Duvall, M. A New Paradigm for Muscle Contraction. *Front. Physiol.* **2015**, *6*, doi:10.3389/fphys.2015.00174.
48. Lillioja, S.; Young, A.A.; Culter, C.L.; Ivy, J.L.; Abbott, W.G.; Zawadzki, J.K.; Yki-Järvinen, H.; Christin, L.; Secomb, T.W.; Bogardus, C. Skeletal Muscle Capillary Density and Fiber Type Are Possible Determinants of in Vivo Insulin Resistance in Man. *J. Clin. Invest.* **1987**, *80*, 415–424, doi:10.1172/JCI113088.
49. Frontera, W.R.; Ochala, J. Skeletal Muscle: A Brief Review of Structure and Function. *Calcif. Tissue Int.* **2015**, *96*, 183–195, doi:10.1007/s00223-014-9915-y.
50. Camman, M.; Marquaille, P.; Joanne, P.; Agbulut, O.; Hélyary, C. Generation of an Adequate Perfusion Network within Dense Collagen Hydrogels Using Thermoplastic Polymers as Sacrificial Matrix to Promote Cell Viability. **2022**, *10*.
51. Urciuolo, A.; Serena, E.; Ghua, R.; Zatti, S.; Giomo, M.; Mattei, N.; Vetralla, M.; Selmin, G.; Luni, C.; Vitulo, N.; et al. Engineering a 3D in Vitro Model of Human Skeletal Muscle at the Single Fiber Scale. *PLOS ONE* **2020**, *15*, e0232081, doi:10.1371/journal.pone.0232081.
52. Hinson, J.T.; Chopra, A.; Lowe, A.; Sheng, C.C.; Gupta, R.M.; Kuppusamy, R.; O'Sullivan, J.; Rowe, G.; Wakimoto, H.; Gorham, J.; et al. Integrative Analysis of PRKAG2 Cardiomyopathy IPS and Microtissue Models Identifies AMPK as a Regulator of Metabolism, Survival, and Fibrosis. *Cell Rep.* **2016**, *17*, 3292–3304, doi:10.1016/j.celrep.2016.11.066.
53. Wang, J.; Zhou, C.J.; Khodabukus, A.; Tran, S.; Han, S.-O.; Carlson, A.L.; Madden, L.; Kishnani, P.S.; Koeberl, D.D.; Bursac, N. Three-Dimensional Tissue-Engineered Human Skeletal Muscle Model of Pompe Disease. *Commun. Biol.* **2021**, *4*, 524, doi:10.1038/s42003-021-02059-4.

## **Supporting Information**

### **Anisotropic dense collagen hydrogels with two ranges of porosity to mimic the skeletal muscle extracellular matrix**

Marie Camman<sup>1,2</sup>, Pierre Joanne<sup>2</sup>, Julie Brun<sup>3</sup>, Alba Marcellan<sup>3</sup>, Julien Dumont<sup>4</sup>, Onnik Agbulut<sup>2\*</sup>, Christophe Hélyary<sup>1\*</sup>

<sup>1</sup> Laboratoire de Chimie de la Matière Condensée de Paris, Sorbonne Université, CNRS, UMR 7574, F-75005, Paris, France.

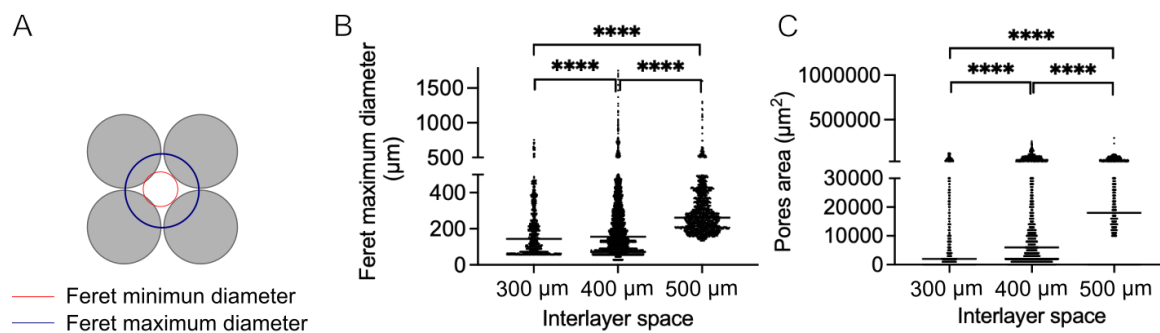
<sup>2</sup> Institut de Biologie Paris-Seine (IBPS), Sorbonne Université, CNRS, UMR 8256, Inserm U1164, Biological Adaptation and Ageing, F-75005, Paris, France.

<sup>3</sup> Sciences et Ingénierie de la Matière Molle, ESPCI Paris, Université PSL, CNRS, Sorbonne Université, F-75005, Paris, France.

<sup>4</sup> CIRB Microscopy facility, Collège de France, CNRS, UMR 7241, Inserm U1050, F-75005, Paris, France.

\* Corresponding authors: Christophe Hélyary and Onnik Agbulut  
Email address : [christophe.helary@sorbonne-universite.fr](mailto:christophe.helary@sorbonne-universite.fr) & [onnik.agbulut@sorbonne-universite.fr](mailto:onnik.agbulut@sorbonne-universite.fr)

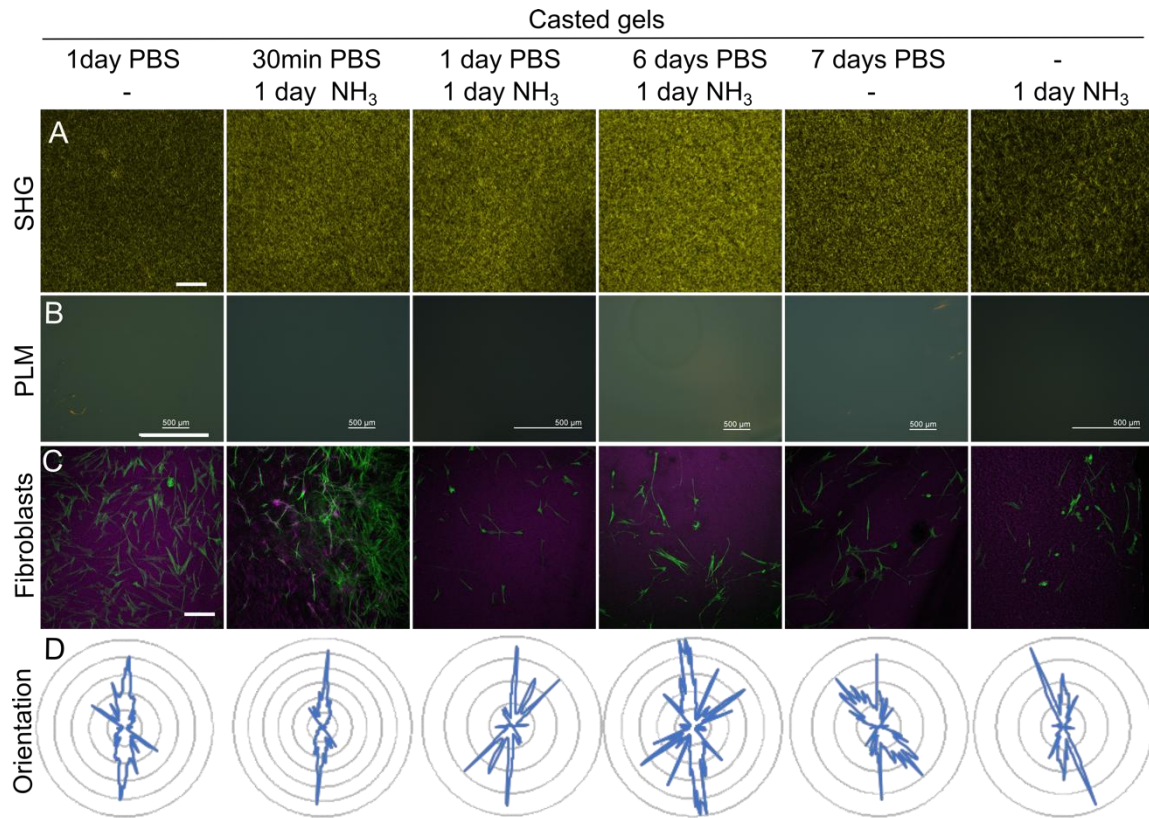
Postal address: Sorbonne University - Campus Pierre et Marie Curie, 4 place Jussieu, 75252 Paris Cedex 05, France





**Figure S1.** A- Determination of Feret diameter to evaluate pore size. B- Feret maximum diameter depending on the interlayer space. C- Pores area depending on the interlayer space.

	0.3 mm	0.4 mm	0.5 mm
Pores mean area ( $\mu\text{m}^2$ )	19440 $\pm$ 26210	23620 $\pm$ 34290	35190 $\pm$ 24770
Feret min ( $\mu\text{m}$ )	114,6 $\pm$ 84,87	127,5 $\pm$ 93,93	187,1 $\pm$ 64,56
Feret max ( $\mu\text{m}$ )	186,7 $\pm$ 137,2	205,5 $\pm$ 162,1	294,8 $\pm$ 139
Circularity	0,8339 $\pm$ 0,1861	0,7797 $\pm$ 0,1976	0,6923 $\pm$ 0,1972
Number of pores	1,719 $\pm$ 1,795	14,11 $\pm$ 7,034	3,203 $\pm$ 1,929

**Figure S2.** Table of numerical results after image analysis.



**Figure S3.** Anisotropy observation and quantification within casted dense collagen hydrogels. (A) Second-harmonic Microscopy Imaging (scale bar 100  $\mu\text{m}$ ). (B) Polarized Light microscopy (scale bar 500  $\mu\text{m}$ ). (C) Fibroblasts alignment on hydrogels. Green: Fibroblasts labeled with Alexa Fluor 488 Phalloidin, Purple: SHG signal from collagen fibrils. (scale bar 250  $\mu\text{m}$ ). (D) Quantification of cell alignment by Orientation J treatment. Percentage of cells depending on the angle they made with the filament orientation ( $0^\circ$ ).

Young's modulus (kPa)	1 day PBS	30 min PBS 1 day NH <sub>3</sub>	1 day PBS 1 day NH <sub>3</sub>	6 days PBS 1 day NH <sub>3</sub>	7 days PBS	1 day NH <sub>3</sub>
<b>Casted</b>	24.5 ± 5.4	13.8 ± 3.5	20.4 ± 4.0	32.8 ± 10.4	26.18 ± 12.5	16.6 ± 4.1
	25.0 ± 9.4	16.3 ± 1.5	25.1 ± 9.6	17.3 ± 9.9	10.8 ± 1.6	16.0 ± 4.2
	8.5 ± 1.9	18.7 ± 1.8	16.0 ± 7.5	13.0 ± 2.9	6.4 ± 0.9	13.0 ± 3.9

**Figure S4.** Young's modulus is calculated on the small deformations for all types of gels.

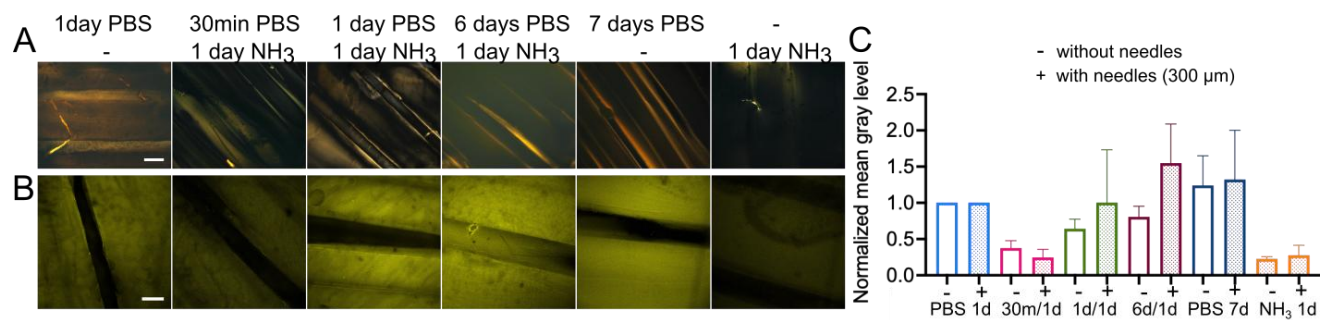


**Figure S5.** Generation of large channels within printed hydrogels without alteration of collagen anisotropy. (A) Polarized light microscopy on 3D-printed hydrogel slices with the presence of needles. (scale bar 500 μm). (B) Second-harmonic generation imaging of slices of printed gels with needles (scale bar 250 μm). (C) SHG intensity of printed hydrogels with needles (+) compared to those without needles (-).



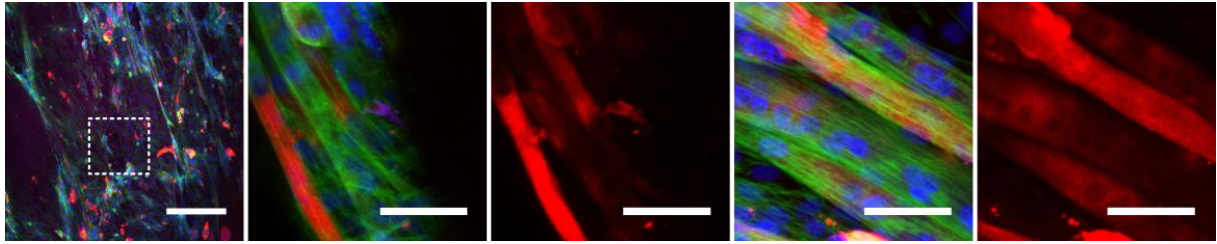


**Figure S6.** C2C12 seeded into printed gels for 7 days. Left: Longitudinal view of large pores (scale bar 100  $\mu\text{m}$ ). Green: actin, blue: nucleus, red: MF20. Zoom on myotubes alignment and myosin staining (scale bar 50  $\mu\text{m}$ ).